Proceedings of ASME Turbo Expo 2010: Power for Land, Sea and Air
GT2010
June 14-18, 2010, Glasgow, UK

GT2010-23300

A CFD STUDY OF LOW REYNOLDS NUMBER FLOW IN HIGH LIFT CASCADES

Roberto Pacciani
Michele Marconcini
Andrea Arnone
"Sergio Stecco" Department of Energy Engineering
University of Florence
via di Santa Marta, 3, 50139 Firenze, Italy
Roberto.Pacciani@unifi.it

Francesco Bertini
Avio S.p.A.
Via I Maggio 99, 10040, Rivalta di Torino (TO), Italy
Francesco.Bertini@aviogroup.com

ABSTRACT

A study of the separated flow in high-lift, low-Reynolds-number cascade, has been carried out using a novel three-equation, transition-sensitive, turbulence model. It is based on the coupling of an additional transport equation for the so-called laminar kinetic energy with the Wilcox k-ω model. Such an approach takes into account the increase of the non-turbulent fluctuations in the pre-transitional and transitional region. Two high-lift cascades (T106C and T108), recently tested at the von Kármán Institute in the framework of the European project TATMo (Turbulence and Transition Modelling for Special Turbomachinery Applications), were analyzed. The two cascades have different loading distributions and suction side diffusion rates, and therefore also different separation bubble characteristics and loss levels. The analyzed Reynolds number values span the whole range typically encountered in aeroengines low-pressure turbines operations. Several expansion ratios for steady inflow conditions characterized by different freestream turbulence intensities were considered. A detailed comparison between measurements and computations, including bubble structural characteristics, will be presented and discussed. Results with the proposed model show its ability to predict the evolution of the separated flow region, including bubble bursting phenomena, in high-lift cascades operating in LP-turbine conditions.

NOMENCLATURE

c	blade chord
k	turbulent kinetic energy
k_ℓ	laminar kinetic energy
ℓ_T	turbulence length scale, $\ell_T = k^{1/2}/\omega$
M	Mach number
R_y	wall-normal-distance Reynolds number, $\sqrt{k}y/\nu$
Re_s	streamwise-distance Reynolds number, $u_\infty s/\nu$
Re_T	turbulent Reynolds number, $k/(\nu\omega)$
Re_{is}	isentropic Reynolds number, $u_{is}c/\nu$
S	mean shear rate $S = \sqrt{2S_{ij}S_{ij}}$
s	blade pitch, curvilinear abscissa
R	transfer term
Tu	turbulence intensity, $Tu = \sqrt{2/3 \cdot k}/u$
u	velocity magnitude
x, y	Cartesian coordinates

Greek

α	flow angle
δ_Ω	shear layer vorticity thickness, $\delta_\Omega = \frac{u_\infty}{2}\left(\frac{\partial u}{\partial y}\right)^{-1}_{\max_y}$
γ	intermittency factor
ν	kinematic fluid viscosity
Ω	vorticity magnitude
ω	specific turbulence-dissipation rate
τ_w	wall shear stress
τ_{ij}	Reynolds stress tensor

Subscripts

0	stagnation
1	inflow
2	outflow
ℓ	laminar
∞	freestream
is	isentropic
M	location of the maximum bubble thickness
R	reattachment point
s	separation point
T	turbulent
w	wall

Acronyms

CFD	Computational Fluid Dynamics
DNS	Direct Numerical Simulation
HL	High-Lift
LKE	Laminar Kinetic Energy
LPT	Low-Pressure Turbine
TATMo	Turbulence and Transition Modeling for Special Turbomachinery Applications
UTAT	Unsteady Transition in Axial Turbines

INTRODUCTION

After several decades of optimization of gas turbines for aero-engines, their upper performance limit in terms of power output and efficiency seems now to be quite close. In the meantime other trends have been superimposed onto design philosophies, pushed by environmental and economic requirements. Such requirements call for lighter jet engine designs, with less components but still with a high efficiency level.

For the low pressure (LP) turbine this leads to a reduction of the number of blades per stage and therefore increased blade loading. Low-pressure turbine blades work with relatively low Reynolds numbers and such flow conditions may be particularly critical for the suction side boundary layer which is responsible for the greatest contribution to the profile loss (up to the 85%). On isolated blade rows, low Reynolds number operations are likely to produce boundary-layer separation in regions of adverse pressure gradient, and important loss enhancements are associated to these circumstances. In the engine multistage environment, the unsteady wake induced transition plays a key role in reducing the separation effects up to a level compatible with acceptably low losses.

Many studies demonstrate how high-lift [1, 2] and ultra-high-lift [3, 4] airfoils can be operated with loss control by taking advantage of wake-induced transition in LPT low-Reynolds-number flows. The study of wake-induced transition in LP turbines has thus led to improvements in performance of present-generation turbomachinery [5, 6]. With a reduction of the suction-side separation effects, now recognized to be the basic mechanism providing increased blade load at acceptably low loss levels, designers and researchers are now looking for other flow-control devices in order to keep supporting and enhancing the high-lift concept.

The control of boundary-layer separation by using active or passive devices represents a promising practice towards the aim of improving the performance of modern high-lift blading of aero-engines LP turbines [7, 8]. To assess the benefits arising from the use of such devices and/or of wake-induced transition, it is important to be able to compute separation bubbles in isolated cascades with steady inflow and hence the resulting loss levels.

Separation bubbles are commonly classified as "short" and "long" [9, 10]. Short bubbles occur at higher Reynolds numbers, and are expected to have only a local effect on the pressure distribution. Transition is triggered by Tollmien-Schlichting (TS) waves originating in the attached boundary layer upstream, and through the development of Kelvin-Helmholtz (KH) instabilities in the separated shear layer. Such instabilities may eventually result in vortex shedding [11, 12], which tends to accelerate reattachment, giving rise to a short bubble. The formation of a long bubble arises predominantly at low Reynolds numbers, and this tends to influence the pressure distribution along the entire blade surface. In this regime, the transition process is slower and turbulent mixing is reduced so that the shear layer is unable to reattach rapidly. The switching of the bubble structure from the short to the long configuration usually occurs in high lift airfoils when decreasing the Reynolds number, and it is usually referred as bursting (see Gaster [9] and Lou and Hourmouziadis [10]). Such a phenomenon occurs in quite a sudden manner when the Reynolds number goes below a certain critical value. The possibility of predicting the occurrence of bursting is crucial to analyze the performance of high lift LP-turbine airfoils. In fact, the associated strong increase in losses could suggest the implementation of passive/active flow control concepts in order to obtain acceptable efficiency levels in practical applications.

Today, turbulence closure in industrial CFD codes are mainly based on one- or two-equation models. However, several studies [13–16] have shown that they can be inefficient, or barely adequate when dealing with flows affected by separation-induced transition mechanisms. A number of approaches have been proposed to address this problem. The majority of the approaches to modelling separated-flow transition are based on the intermittency concept. This concept provides a fairly general framework for any transition mechanism – be it of the natural, bypass, separated-flow or unsteady wake-induced type – to be modelled.

Suzen et al. [16] have formulated a transport equation for the intermittency factor to predict transitional flows in low-pressure turbines. Menter et al. [13] have coupled an intermittency and a transition-onset Reynolds number transport model to obtain a dynamic description of the transition, which makes use of local variables only. In particular, as done also by other authors [15], they have adopted intermittency distributions that exceed unity inside the separated flow region. This strategy allows the turbulence production to react quickly to transition, thus compensating for the deficiency of eddy-viscosity models discussed above and ensuring the prediction of realistic reattachment locations. On the other hand, intermittency formulations rely, at least to some degree, on non-local quantities, even when embedded in transport models. Furthermore, they have to be coupled to a transition-onset criterion, which is again often based on non-local flow quantities.

More recent methodologies, that are based on the concept of the transport of laminar kinetic energy (LKE), are theoretically more general, i.e. they do not rely on global quantities or correlations. Walters and Leylek [17, 18] and Lardeau et al. [19] exploited the LKE concept, originally introduced by Mayle and Schulz [20], to sensitize a two-equation model to the onset of natural and bypass transition. They are essentially characterized by conventional transport models that can readily be formulated in terms of local flow quantities. They are able to address the rise of pre-transitional fluctuations in boundary layers and their subsequent breakdown to turbulence. Examples of successful applications of the LKE approach to LP turbines has been provided by Lardeau and Leschziner [21] and by Pacciani et al. [22].

The present paper assesses the application of a new LKE model to the calculation of high-lift cascades tested in LP turbine conditions. The gradual rise of pre-transitional fluctuating energy in the separated region is modelled using a new production term based on the mean shear rate and a *laminar eddy-viscosity* concept. The fluctuating energy is then gradually transferred to the turbulence field via a newly derived transfer term. Finally, the LKE model is coupled to the low turbulent Reynolds number formulation of the Wilcox $k-\omega$ model [23] . The well-known T106 and the T108 cascades are used to assess the ability of the present model to predict transitional low-Reynolds-number flows around LP turbine blades. Such high-lift cascades have recently been tested experimentally at the von Kármán Institute within the framework of two European research projects (UTAT and TATMo). The results of the numerical investigations are discussed with reference to a broad range of flow conditions, with different Reynolds numbers, expansion ratios, and freestream turbulence intensities. Particular emphasis will be devoted to the discussion of the capabilities of the present approach to predict the occurrence of bubble-bursting phenomena.

COMPUTATIONAL FRAMEWORK

The Flow Solver

The TRAF code (Arnone et al. [24]) was used in the present work. The unsteady, three-dimensional, Reynolds-averaged Navier-Stokes equations are written in conservative form in a curvilinear, body-fitted coordinate system and solved for density, absolute momentum components, and total energy. A dual-time-stepping method [25, 26] is used to perform time accurate calculations.

Transition and Turbulence Modelling

The proposed model, denoted as LKE model hereafter, is based on the laminar kinetic energy concept of Mayle and Schulz [20], which enables to take into account the pre-transitional rise of the fluctuating kinetic energy. The modelled transport equation for the LKE is written as (Lardeau et al. [19], Pacciani et al. [22]):

$$\frac{Dk_\ell}{Dt} = P_\ell - 2\nu\frac{k_\ell}{y^2} + \nu\nabla^2 k_\ell \tag{1}$$

In attached and separated shear layers, the amplification of fluctuations is due more to conventional shear-stress/strain interaction (Lardeau et al. [27]) rather than to pressure diffusion (Mayle and Schulz [20]). Hence, a model of the production of the laminar kinetic energy can be formulated as follows:

$$P_\ell = \nu_\ell S^2 \tag{2}$$

where ν_ℓ is the *laminar eddy-viscosity*, and is modelled as follows:

$$\nu_\ell = C_1 f_1 \sqrt{k_\ell}\delta_\Omega \tag{3}$$

with $C_1 = 0.01$ deduced from calibration, and:

$$f_1(Tu) = \max\left[0.8, 2.0\cdot\tanh\left[\left(\frac{Tu}{4.5}\right)^{\frac{1}{2}}\right]\right] \tag{4}$$

Once the laminar kinetic energy is created in the separated shear layer, it must be transferred to the turbulence field to trigger the transition process, as shown by numerical [28] and experimental investigations [11]. The laminar and turbulent kinetic energy equation can be written in a general form as follows:

$$\frac{Dk_\ell}{Dt} = P_\ell - 2\nu\frac{k_\ell}{y^2} + \nu\nabla^2 k_\ell - R \tag{5}$$

$$\frac{Dk}{Dt} = P_k - \beta^* k\omega + \frac{\partial}{\partial x_j}\left[(\nu + \sigma_k \nu_T)\frac{\partial k}{\partial x_j}\right] + R \tag{6}$$

where $\beta^* = 0.09$, and P_k is the turbulence-production term:

$$P_k = \tau_{ij}\frac{\partial u_i}{\partial x_j} \tag{7}$$

The term R appears in both equations, but with opposite signs, resulting in no net change of the total fluctuating kinetic energy $k_{tot} = k_\ell + k$. Rather there is a transfer of energy from k_ℓ to k. Following Walters and Leylek [17], this term is assumed to be proportional to k_ℓ:

$$R = C_2 f_2 \omega k_\ell \tag{8}$$

The damping function f_2 is defined as follows:

$$f_2 = 1 - e^{-\psi/C_3} \tag{9}$$

$$\psi = \max\left(0; R_y - C_4\right) \tag{10}$$

The constants are $C_2 = 0.3$, $C_3 = 8$ and $C_4 = 10$. The quantity ψ can be considered as a transition parameter, because it controls the transfer of energy from the laminar to the turbulent state, which occurs when the Reynolds number R_y reaches the threshold value C_4.

The LKE model is then applied in combination with the classical Wilcox low-Reynolds number $k-\omega$ model [23], which is widely used in turbomachinery calculations.

The inlet conditions for k and ω are obtained from the prescribed values of freestream turbulence intensity $k_\infty = 3/2\cdot Tu_\infty^2\cdot u_\infty^2$, and turbulence length scale $\omega_\infty = k_\infty^{1/2}/\ell_{T\infty}$. The inlet condition for k_ℓ is as follows: $k_{\ell\infty} = k_\infty$ (see Mayle and Schulz [20] for more details). At the solid walls the boundary value of ω is computed according to Menter [29]:

$$\omega_w = 800\frac{\mu_w}{\rho_w(\Delta y)^2} \tag{11}$$

where Δy is the grid spacing at the wall.

THE T106C TURBINE CASCADE

The T106 blade section [30] is a widely used geometry for both experimental and numerical studies on high-lift LP profiles. Detailed experimental data are available for a range of incidence, cascade solidity and Reynolds number. The main flow conditions analyzed in the calculations are summarized in Tab. 1.

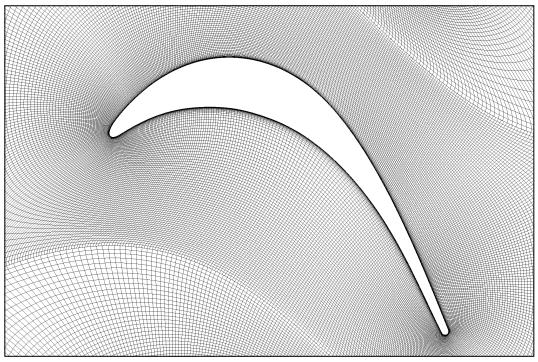

Figure 1: T106C – single-block O-type grid 593×97.

TABLE 1: Main flow parameters for the T106C cascade.

α_1	32.7°
s/c	0.95
M_{2is}	0.6 ; 0.65 ; 0.7
$\ell_{T\infty}/c_x$	2.5×10^{-3}
Tu_∞	0.80%; 1.8%; 2.6%

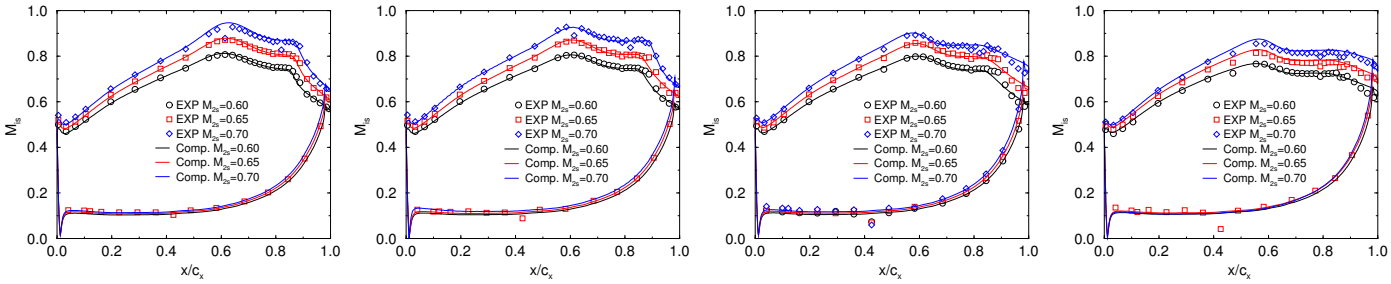

(a) $\mathbf{Re_{2,is} = 1.6 \cdot 10^5}$ **(b)** $\mathbf{Re_{2,is} = 1.2 \cdot 10^5}$ **(c)** $\mathbf{Re_{2,is} = 1.0 \cdot 10^5}$ **(d)** $\mathbf{Re_{2,is} = 0.8 \cdot 10^5}$

Figure 2: T106C cascade: isentropic Mach-number distributions ($\mathbf{Tu_\infty = 0.8\%}$).

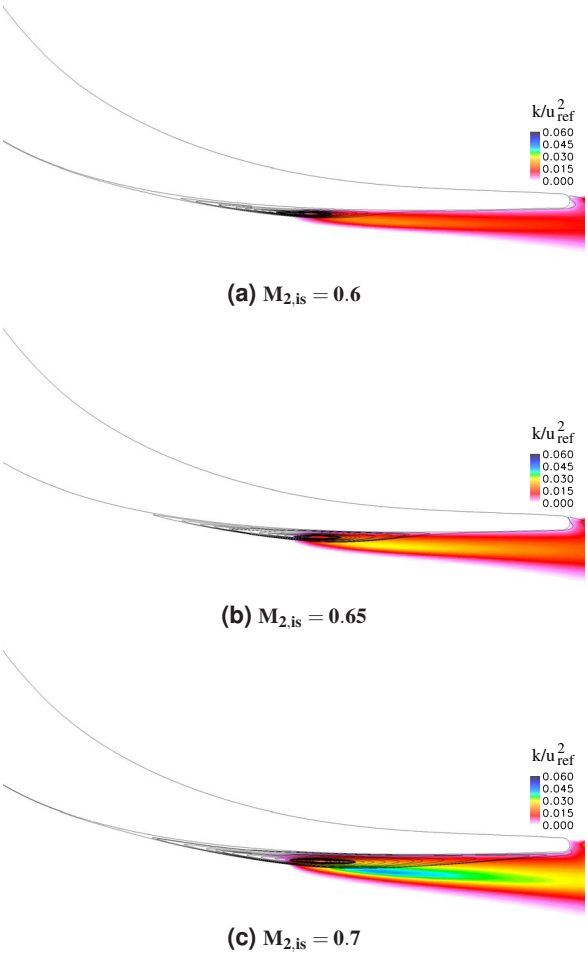

(a) $\mathbf{M_{2,is} = 0.6}$

(b) $\mathbf{M_{2,is} = 0.65}$

(c) $\mathbf{M_{2,is} = 0.7}$

Figure 3: T106C cascade: separation bubble configurations at different exit isentropic Mach numbers for $\mathbf{Re_{2,is} = 1.2 \cdot 10^5}$ ($\mathbf{Tu_\infty = 0.8\%}$).

The 593×97 non-periodic O-type mesh for the T106C cascade shown in shown in Fig. 1. The mesh size was selected on the base of previous grid-dependence analyses [31]. About 40 cells lie inside laminar portions of boundary layers and the y^+ values of the mesh nodes closest to the wall are below unity in turbulent regions.

Several Reynolds number values, ranging from $0.8 \cdot 10^5$ to $2.5 \cdot 10^5$ were investigated. Detailed numerical analyses carried out at low freestream turbulence intensities and for the nominal exit isentropic Mach number $M_{2,is} = 0.65$, are discussed in Pacciani et al. [22]. In the present paper the performance of the proposed $k_\ell - k - \omega$ model is assessed on a broader range of conditions. Such conditions include different cascade expansion ratios and inlet turbulence intensities.

The discussion of the numerical results will be splitted in two subsections. The first will be devoted to the analysis of the effects of the expansion ratio, while in the second the impact of the freestream turbulence level will be examined.

Effects of the expansion ratio

Three-different expansion ratios, leading to exit isentropic Mach number values of $M_{2,is} = 0.6$, 0.65, 0.7 were considered. The corresponding isentropic Mach number distributions on the blade surface, for four different values of the Reynolds number, are compared to experiments in Fig. 2. Measured data have been obtained with a freestream turbulence level of $Tu_\infty = 0.8\%$. The agreement is seen to be very good for all the cases. In particular, the effects of the separation on the isentropic Mach-number distribution are correctly reproduced by the calculations, and small discrepancies arise only at the lower Reynolds numbers, in the pressure-recovery region of the bubble. Here, the calculations tend to predict a slightly smoother pressure gradient with respect the the experiments (Fig. 2(c), 2(d)). For a given Reynolds number, the increase of the exit Mach number results in an increase of the separation-related effects. This indicates that the bubble is growing with the exit Mach number itself.

In the range between $Re_{2,is} = 2.5 \cdot 10^5$ and $Re_{2,is} = 1.2 \cdot 10^5$, the separated flow region appears to have the structure of a short bubble for all the investigated expansion ratios. The situation is quite different at $Re_{2,is} = 1.2 \cdot 10^5$, as it can be deduced from Fig.3, which reports streamlines superposed to turbulent kinetic energy contours in the separated flow region, for the three considered expansion ratios. The cases corre-

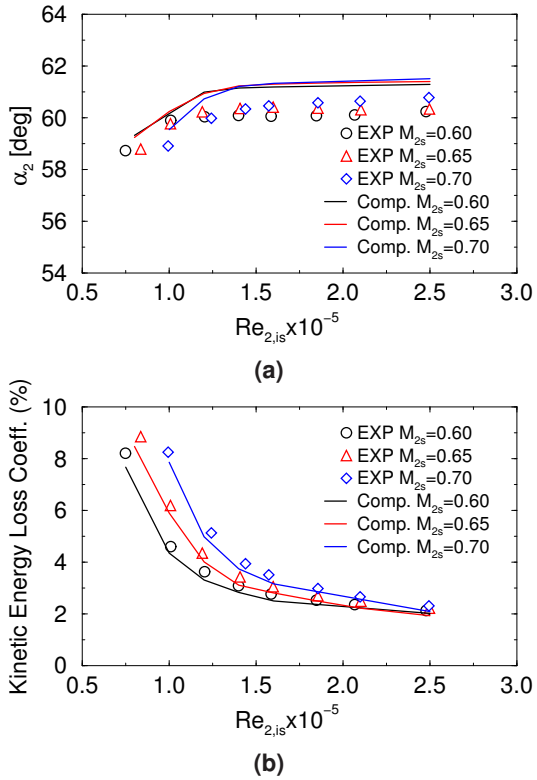

Figure 4: T106C cascade: (a) Exit flow angle (b) Kinetic energy loss coefficient (%) as a function of $Re_{2,is}$ ($Tu_\infty = 0.8\%$).

sponding to $M_{2,is} = 0.6$, $M_{2,is} = 0.65$ are still characterized by a typical short bubble configuration, with the center of the reverse-flow vortex located much closer to the reattachment point than to the separation point, and with evidence of a strong slope of the dividing streamline between the maximum thickness and the reattachment point. On the contrary, the case with highest expansion ratio shows the occurrence of bubble bursting as can be noticed in Fig.3(c). The relevant increase in length of the separated flow region, produced by the displacement of the reattachment location towards the trailing edge, moves the flow configuration into the domain of long bubbles. Transition occurs in harmony with the location of maximum bubble thickness, and this increases with the exit Mach number. As a consequence, the maximum turbulent energy production in the breakdown region occurs at increasing distance from the wall and, at the highest expansion ratio, the resulting turbulence field is not effective for producing a rapid reattachment.

The substantial modification in the blade-load distribution, observable for $Re_{2,is} \leq 1.0 \cdot 10^5$, relative to the cases at the higher Reynolds numbers, suggests that the separated flow region has become a long bubble for all the considered expansion ratios. Indeed, the flow is not even reattached in the case at the lowest Reynolds number ($Re_{2,is} = 0.8 \cdot 10^5$), indicating the presence of an open separation rather than a long bubble.

The appearance of bubble bursting is generally associated to Reynolds number values which are below a certain critical value. Such a value is then predicted to occur between $Re_{2,is} = 1.2 \cdot 10^5$ and $Re_{2,is} = 1.0 \cdot 10^5$ for the present blade, and it is found to increase when increasing the cascade expansion ratio.

The correct prediction of the phenomena associated to bursting can also be assessed from the lapse-rates of Fig. 4. Here the computed exit flow angle and kinetic energy loss coefficient as a function of $Re_{2,is}$ are compared to the corresponding measured data. The agreement is remarkable on the whole range of investigated conditions. The difference between the computed and experimental flow angle is about 1.0°, while losses are only mildly underestimated at low Reynolds numbers. The exit flow angle remains almost constant for Reynolds number values which are above the critical one. For $Re_{2,is}$ below this value, the exit flow angle rapidly decreases. Both computed and experimental loss coefficients undergo an abrupt increase in their rates of change in the critical range of the Reynolds number, and consistently with the previous observations, such an increase occurs at higher Reynolds numbers for higher expansion ratios.

Figure 5 compares calculated and measured distributions of total pressure defect ($(p_{01} - p_0)/p_{01}$) along a traverse taken at $0.45 \cdot c_x$ downstream the blade trailing edge. Such a comparison is reported for three different values of the Reynolds number, and for $M_{2,is} = 0.65$. The experimental wake total pressure profile is well reproduced by the calculations at the higher Reynolds numbers (Fig. 5(a)), while discrepancies begin to appear around $Re_{2,is} = 1.2 \cdot 10^5$ and tend to become more pronounced below this value (Figures 5(b)- 5(c)). In particular, a deeper and narrower profile is predicted at low Reynolds numbers, and such a circumstance is typically associated to an underestimation of the turbulent diffusion in the wake region (e.g. Menter [29, 32, 33], Wilcox [23]). Since most important contributions to mass-flow averaged quantities come from regions of higher velocity, the narrower wake profile could be associated to the aforementioned loss underestimation for $Re_{2,is} < 1.2 \cdot 10^5$ (Fig. 4(b)).

When analyzing wake details at relevant distances downstream the trailing edge, a certain lack of diffusivity is quite common in RANS analyses of turbomachinery bladings carried out with linear eddy viscosity models (e.g. Chima [34]). However, in the present case, this seems to be a distinct feature of the low Reynolds number regime. An explanation for this fact can be attempted on the base of the following arguments. The growth of the laminar kinetic energy in the pre-transitional separated shear-layer mimics some effects of the flow instabilities developing in this region. The energy transfer term of equation 8 drives the growth of the turbulent quantities in the breakdown region. In the Reynolds number regime, which is dominated by the presence of long bubbles, flow structures developing on larger scales than those which are modelled via the $k_\ell - k - \omega$ approach (like vortex pairing, shedding, etc.) are known to occur [35] and influence the near-wall layer, the wake structure, and the related loss levels. The prediction of the effects of such phenomena could be beyond the capabilities of the proposed modelling framework and perhaps of steady RANS approaches in general.

Effects of the freestream turbulence

A freestream turbulence increase results in a reduction of the extension of the separated flow region [36]. For the T106C cascade the most pronounced effects were recorded for $Re_{2,is} < 0.8 \cdot 10^5$. The isentropic Mach number distributions, obtained with three different freestream turbulence intensities ($Tu_\infty = 0.8\%$, 1.8%, 2.6%), are reported for the case with $Re_{2,is} < 0.8 \cdot 10^5$ and $M_{2,is} = 0.65$ in Fig. 6. Such a case shows

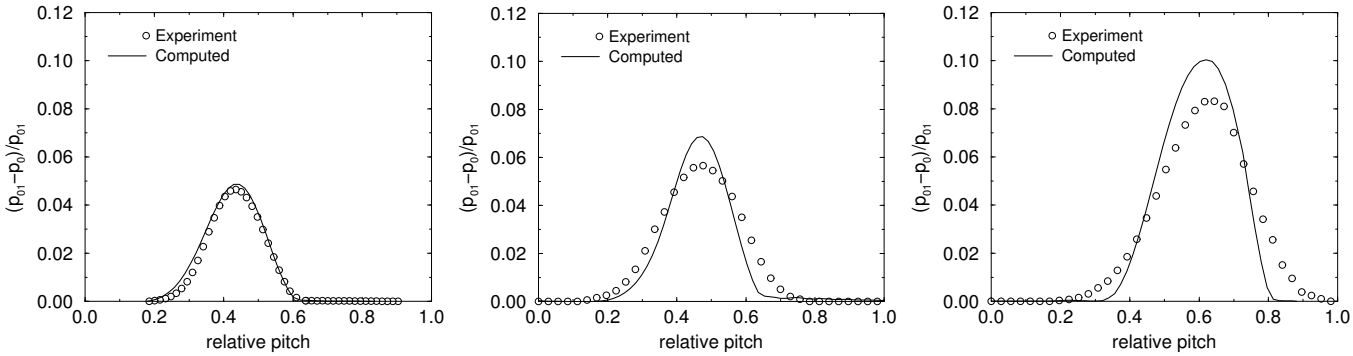

(a) $\mathbf{Re_{2,is} = 2.5 \cdot 10^5}$ **(b)** $\mathbf{Re_{2,is} = 1.2 \cdot 10^5}$ **(c)** $\mathbf{Re_{2,is} = 0.8 \cdot 10^5}$

Figure 5: T106C cascade: wake total pressure defect profiles ($\mathbf{x/c_x = 1.45}$, $\mathbf{M_{2,is} = 0.65}$, $\mathbf{Tu_\infty = 0.8\%}$).

the most significant impact of the freestream turbulence level, and thus, for the sake of conciseness, it is the only one that will be discussed here in terms of blade loading distributions. The agreement between computed and experimental results is again remarkable for the investigated conditions.

Increasing the freestream turbulence level for $Tu_\infty = 0.8\%$ to $Tu_\infty = 1.6\%$ results in a strong contraction of the separated flow region. The open separation that exists for $Tu_\infty = 0.8\%$ becomes a long bubble at higher freestream turbulence intensities. Such a circumstance can be deduced from the isentropic Mach number distributions of Fig. 6 that show the evidence of a late reattachment for $Tu_\infty = 1.8\%$. A further increase in the freestream turbulence intensity only results in a much weaker effect on the separated flow region, with small reductions of its extension and no appreciable change in structure. Although not reported, similarly weak effects on the isentropic Mach number distribution were detected for $Re_{2,is} > 1.2 \cdot 10^5$ and they were confirmed by the experimental findings [36].

As far as bubble bursting is concerned, the increase in the freestream turbulence level was also found to be responsible for a decrease of the critical Reynolds number. Such a circumstance can be appreciated in Fig. 7, where lapse rates are reported for the investigated Tu_∞ values. A strong reduction of the kinetic energy loss coefficient occurs for $Re_{2,is} < 1.2 \cdot 10^5$ when increasing the Tu_∞ value from $Tu_\infty = 0.8\%$ to $Tu_\infty = 1.8\%$. This is associated to the contraction of the separation bubble extension, indicating that bubble bursting occurs for lower values of the Reynolds number. Only minor changes are associated with the further increase of the turbulence level to the value of $Tu_\infty = 2.6\%$.

The beneficial effect of the freestream turbulence is correctly captured by the calculations, even if the difference in losses, between the two higher Tu_∞ values is predicted to be mildly less pronounced than in the experiments. In fact, while computed the kinetic energy loss coefficient agrees well with the measured one at $Tu_\infty = 1.8\%$, it is somehow overestimated at $Tu_\infty = 2.6\%$ at low Reynolds number conditions.

Similar considerations hold for the exit flow angle. When increasing Tu_∞, the abrupt decrease for $Re_{2,is} < 1.2 \cdot 10^5$ tends to disappear and a less pronounced and gradual reduction of the exit flow angle is

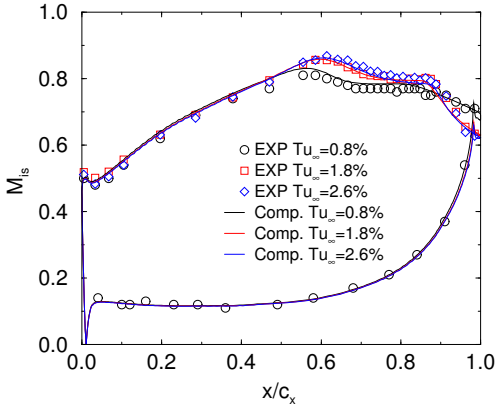

Figure 6: T106C cascade: isentropic Reynolds number distributions for different freestream turbulence levels ($\mathbf{Re_{2,is} = 0.8 \cdot 10^5}$, $\mathbf{M_{2,is} = 0.65}$).

instead experienced when lowering Reynolds numbers. Again this trend is correctly captured by calculations and it was found to be related to the contraction of the separation bubble, which is associated to a reduction of flow underturning.

Hatman and Wang [11] devised correlations for the maximum bubble displacement and reattachment locations as a function of the local Reynolds number at the separation point. With no experimental result available on the structure of the separated region, the present numerical predictions are compared to the Hatman and Wang correlations [11] in order to gain enhanced insight into the physical aspects of the computed bubble structure.

The comparisons are reported in Fig. 8(a) and 8(b), in terms of Reynolds number at the maximum bubble thickness and reattachment locations, as a function of the separation Reynolds number. The computed results for $Tu_\infty = 0.8\%$ are substantially coincident with the Hatman and Wang predictions for all the considered expansion ratios. The results obtained with $Tu_\infty = 1.8\%$ and $Tu_\infty = 2.6\%$ also exhibit a

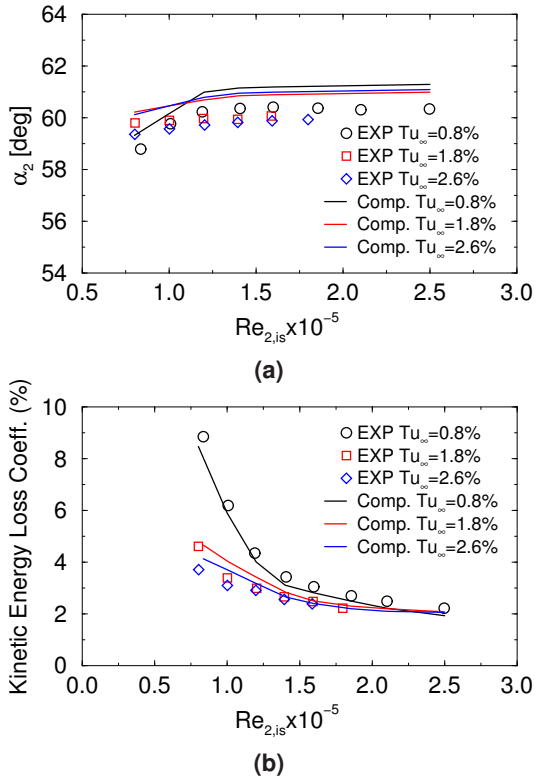

Figure 7: T106C cascade: (a) Exit flow angle and (b) Kinetic energy loss (%) as a function of $Re_{2,is}$ for different freestream turbulence levels ($M_{2,is} = 0.65$).

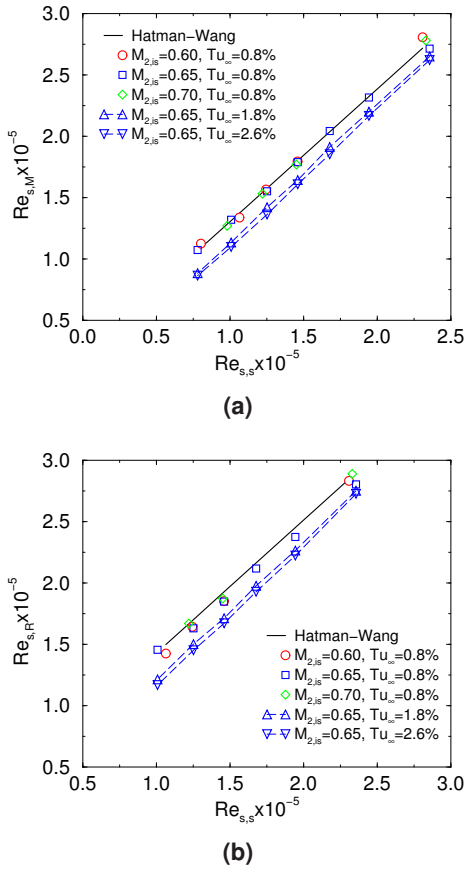

Figure 8: T106C cascade: Local Reynolds number at (b) maximum separation bubble thickness location and (b) reattachment compared with Hatman and Wang [11].

linear behavior, with a slope which is slightly higher than the one of the correlation. Both the maximum bubble thickness and reattachment locations are predicted to be upstream relative to the correlation results. Such a fact is not surprising if we consider that the freestream turbulence intensity is not accounted for in the Hatman and Wang correlation, and it is consistent with the discussed effects concerning the reduction of the separation extension.

The comparison of Figures 8(a) and 8(b) indicates that, in the considered conditions in terms of exit Mach number and inlet turbulence level, the evolution of the separation bubble structure with the Reynolds number is correctly reproduced by the proposed approach.

THE T108 TURBINE CASCADE

The T108 cascade is a high-lift configuration, which was tested experimentally at the von Kármán Institute as part of the TATMo research project. The airfoil geometry and the 593×97, non-periodic O-Type grid used for the calculations are shown in Fig. 9. The T108 airfoil is front loaded and, with respect to T106C cascade, it shows a much gradual diffusion from the suction velocity peak to the blade trailing-edge. At all the Reynolds numbers, separation bubbles occurring on the blade suction-side were then expected to be smaller than in the previous case.

Experiments were conducted for an exit isentropic Mach number

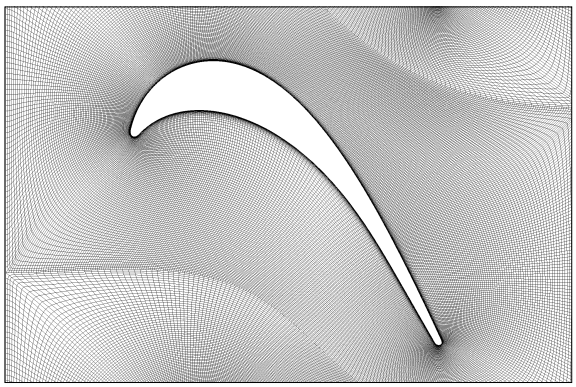

Figure 9: T108 – single-block O-type grid 593×97.

value of $M_{2,is} = 0.6$, and the tested Reynolds number values range from $Re_{2,is} = 0.7 \cdot 10^5$ to $Re_{2,is} = 2.0 \cdot 10^5$. The main flow conditions analyzed in the calculations are summarized in Tab. 2.

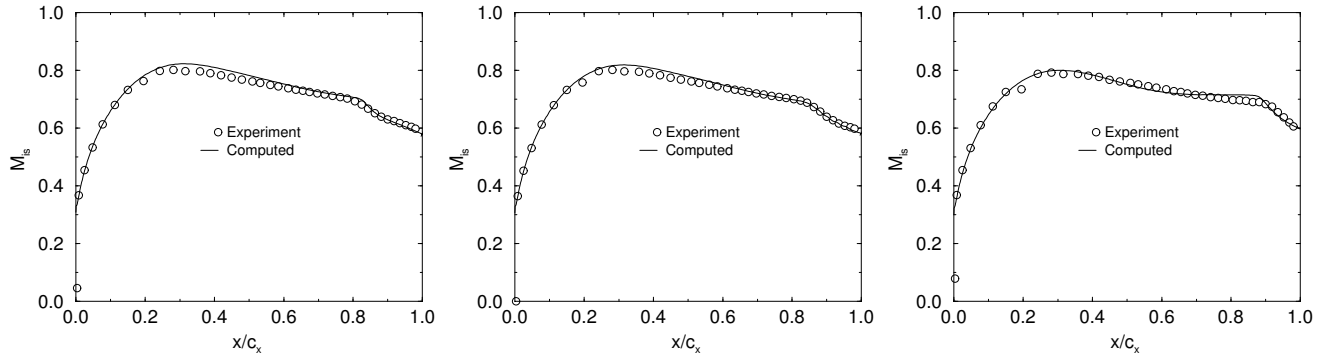

(a) $\mathbf{Re_{2,is} = 2.0 \cdot 10^5}$ **(b)** $\mathbf{Re_{2,is} = 1.4 \cdot 10^5}$ **(c)** $\mathbf{Re_{2,is} = 0.7 \cdot 10^5}$

Figure 10: T108 cascade: isentropic Mach-number distribution.

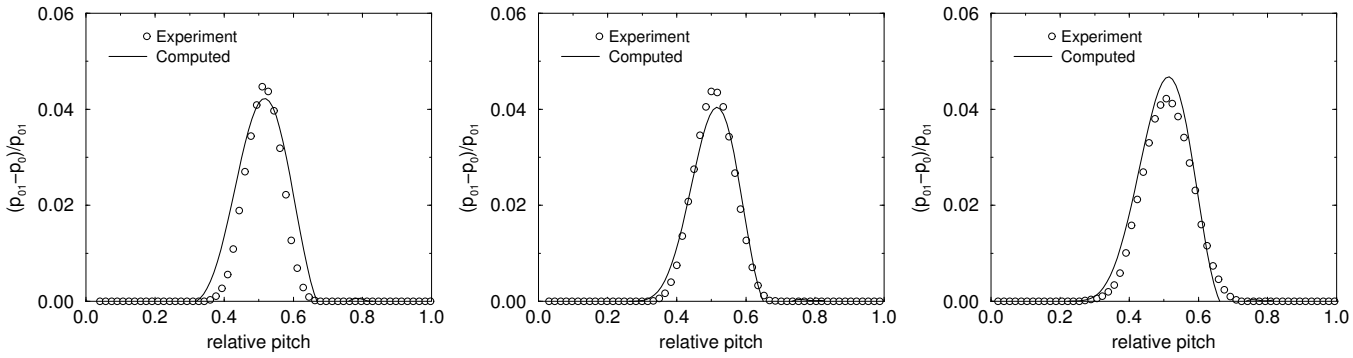

(a) $\mathbf{Re_{2,is} = 2.0 \cdot 10^5}$ **(b)** $\mathbf{Re_{2,is} = 1.4 \cdot 10^5}$ **(c)** $\mathbf{Re_{2,is} = 0.7 \cdot 10^5}$

Figure 11: T108 cascade: total pressure defect downstream the trailing edge ($\mathbf{x/c_x = 1.45}$).

Figure 10 compares calculated and measured isentropic Mach number distributions along the blade suction side for three different values of the Reynolds number. They suggest that the suction side boundary layer appears to be mildly separated at the highest Reynolds number, and that the separated flow region has still the structure of a very small bubble even at the lowest Reynolds number.

The separation impact on the suction side isentropic Mach number distribution is seen to increase as the Reynolds number decreases, but it appears to have only a local effect, without overall modifications of the distribution itself. This indicates that the occurrence of bubble bursting is delayed to even lower Reynolds numbers for this blade. The agreement between computations and experiments is very good. Minor discrepancies can only be observed in the laminar portion of the bubble, approximately between the 65% and the 80% of the axial chord, where the computations tend to predict a more pronounced velocity plateau with respect to the measured one. As can be observed, those differences tend to become more evident at the lowest Reynolds number (Fig. 10(c)). Such a circumstance suggests a correspondingly slight overestimation of the blockage and consequently of the bubble thickness. On the contrary, the bubble length seems to be very well reproduced by the computations and also the pressure recovery rate corresponding to the turbulent portion of the bubble is correctly predicted.

TABLE 2: Main flow parameters for the T108 cascade.

α_1	34.7°
s/c	1.05
M_{2is}	0.60
$\ell_{T\infty}/c_x$	2.5×10^{-3}
Tu_∞	1.00%

Although not reported in this paper, the computed bubble characteristics, in terms of maximum thickness and reattachment locations as a function of the Reynolds number, were again found to be in substantial agreement with the predictions of the Hatman and Wang correlation.

The pitchwise total pressure deficit distributions in the wake region also compare well with the experiments as shown in Fig. 11. Only

a slightly deeper defect is predicted by the calculations for the lower Reynolds number.

Computed lapse rates are compared to experimental ones in Fig. 12. Despite some scattering in the measured exit flow angles, which is not detected in the calculations (Fig. 12(a)), on the average the agreement can be regarded as satisfactory. In particular, both experimental and calculated values show a very gradual decrease when decreasing the Reynolds number in the considered range. Such a behavior is quite different from the one experienced for the T106C cascade and is consistent with the gradual increase of the separation bubble, without bursting phenomena, found for the present cascade.

Similar considerations hold for the kinetic energy loss coefficient as a function of the Reynolds number (Fig. 12b). The gradual loss increase for decreasing Reynolds number shown by the experimental results is very well reproduced by the computations and no abrupt loss raise due to the appearance of a long bubble can here be appreciated. It can also be noticed how the loss level is clearly below the one of the T106C cascade, especially at low Reynolds number. As reported by other authors [37], this is expected to be the result of the different loading distributions of the two high-lift blades. In particular, for a same value of the cascade solidity, a front loaded design produces a smoother adverse pressure gradient in the diffusing region of the blade suction side. This, not only results in smaller separation bubbles, but it also displaces the occurrence of bursting below the Reynolds number range of interest in practical applications.

Again minor discrepancies appear between experimental and computed results at the the lower Reynolds number values ($Re_{2,is} < 1.0 \cdot 10^5$), where the kinetic energy loss coefficient is slightly overestimated by the calculations (Fig. 12(b)). Some scattering is detectable in the measurements, and indeed the differences are below the 1% of the experimental values.

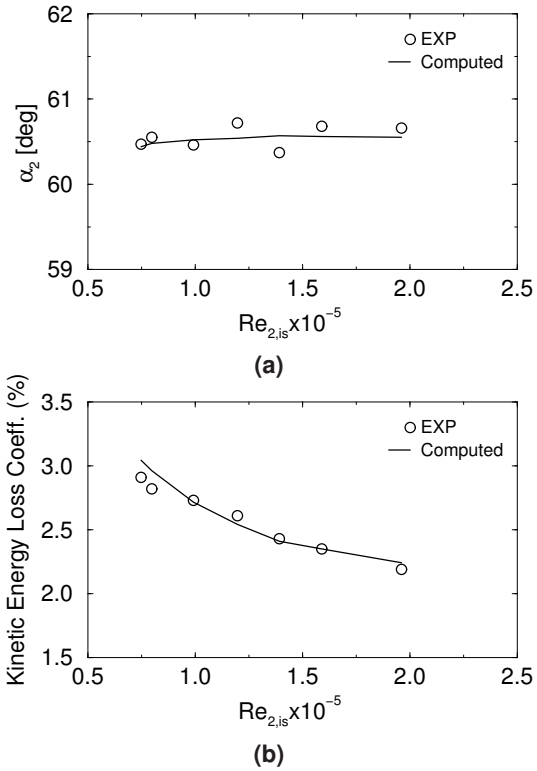

Figure 12: T108 cascade: kinetic energy loss (%) and exit flow angle as a function of $Re_{2,is}$.

CONCLUDING REMARKS

A new model, based on the laminar kinetic energy concept originally introduced by Mayle and Schulz [20], is coupled to a linear eddy-viscosity model to predict separated-flow transition in high-lift cascades operating in conditions representative of those in low-pressure turbines.

The novel $k_\ell - k - \omega$ model displays very good performance when applied to the T106C and T108 cascades. The assessment covered a range of Reynolds numbers, expansion ratios, and freestream turbulence levels, within which short as well as long separation bubbles are produced on the blade suction side. The inception of bubble bursting, in the cases it occurs, is correctly predicted, together with its effects on blade loading distributions and lapse rates. However underestimated diffusion can be expected in large wakes arising from long bubbles or open separations. The validity of the computations is reinforced by a favorable comparison of some structural features of the separation bubbles with the classical results of Hatman and Wang [11].

The study may be claimed to have demonstrated that the proposed model offers an economical and accurate mean of providing affordable engineering predictions of transitional flows in LP turbines, even if a somewhat weaker performance is shown in the very low Reynolds number regime. This is the range of conditions were unsteady flow structure develop on spatial scales that undergo a questionable modelling in the framework of RANS approaches using simple linear eddy-viscosity closures. Fundamental investigations, carried out with approaches that are able to resolve the physical details, and therefore the effects of such structures (i.e. LES or DNS), could be of great help in suggesting further modelling ideas to support and enhance transition-sensitive turbulence closures.

ACKNOWLEDGMENTS

The research reported in this paper was undertaken within the European Commission research project TATMo (AST5-CT-2006-030939, `www.tatmo.eu`). Part of the experimental data were obtained within the research project UTAT (G4RD-CT-2001-00628) funded by the European Commission. We would like to thank our fellow partners in European Union FP6 programme TATMo for permitting the publication of our results in this paper.

REFERENCES

[1] Cobley, K., Coleman, N., Siden, G., and Arndt, N., 1997, "Design of New Three Stage Low Pressure Turbine for the BMW Rolls-Royce BR715 Turbofan Engine". ASME paper 97–GT–419.

[2] Curtis, E. M., Hodson, H. P., Banieghbal, M. R., Denton, J. D., Howell, R. J., and Harvey, N. W., 1997, "Development of Blade Profiles for Low Pressure Turbine Applications". ASME J. Turbomach., **119** (3), pp. 531–538.

[3] Haselbach, F., Schiffer, H. P., Horsman, M., Dressen, S., Harvey, N. W., and Read, S., 2002, "The Application of Ultra High Lift Blading in the BR715 LP Turbine". ASME J. Turbomach., **124** (1), pp. 45–51.

[4] Howell, R. J., Hodson, H. P., Schulte, V., Stieger, R. D., Schiffer, H. P., Haselbach, F., and Harvey, N. W., 2002, "Boundary Layer Development in the BR710 and BR715 LP Turbines – The Implementation of High–Lift and Ultra–High–Lift Concepts". ASME J. Turbomach., **124** (3), pp. 385–392.

[5] Schulte, V. and Hodson, H. P., 1998, "Unsteady Wake–Induced Boundary Layer Transition in High Lift LP Turbines". ASME J. Turbomach., **120** (1), pp. 28–35.

[6] Stieger, R. D. and Hodson, H. P., 2004, "The Transition Mechanism of Highly Loaded Low-Pressure Turbine Blades". ASME J. Turbomach., **126** (4), pp. 536–543.

[7] Zhang, F. H., Vera, M., Hodson, H. P., and Harvey, N., 2006, "Separation and Transition Control on an Aft-Loaded Ultra-High-Lift LP Turbine Blade at Low Reynolds Numbers: Low-Speed Investigation". ASME J. Turbomach., **128** (3), pp. 517–527.

[8] Rumsey, C. L., Gatski, T. B., Sellers III, W. L., Vatsa, V. N., and Viken, S. A., 2006, "Summary of the 2004 Computational Fluid Dynamics Validation Workshop on Synthetic Jets". AIAA J., **44** (2), pp. 194–207.

[9] Gaster, M., 1969, "The Structure and Behaviour of Laminar Separation Bubbles". Aeronautical Research Council R&M 3595.

[10] Lou, W. and Hourmouziadis, J., 2000, "Separation Bubbles Under Steady and Periodic-Unsteady Main Flow Conditions". ASME J. Turbomach., **122** (4), pp. 634–643.

[11] Hatman, A. and Wang, T., 1999, "A Prediction Model for Separated-Flow Transition". ASME J. Turbomach., **121** (3), pp. 594–602.

[12] McAuliffe, B. R. and Yaras, M. I., 2005, "Separation-Bubble-Transition Measurements on a Low-Re Airfoil Using Particle Image Velocimetry". ASME paper GT2005–68663.

[13] Menter, F. R., Langtry, R. B., Likki, S. R., Suzen, Y. B., Huang, P. G., and Völker, S., 2006, "A Correlation-Based Transition Model Using Local Variables – Part I: Model Formulation". ASME J. Turbomach., **128** (3), pp. 413–422.

[14] Langtry, R. B., Menter, F. R., Likki, S. R., Suzen, Y. B., Huang, P. G., and Völker, S., 2006, "A Correlation-Based Transition Model Using Local Variables – Part II: Test Cases and Industrial Applications". ASME J. Turbomach., **128** (3), pp. 423–434.

[15] Kožulović, D., Röber, T., and Nürnberger, D., 2007, "Application of a Multimode Transition Model to Turbomachinery Flows". 7th European Turbomach. Conf., Athens, Greece.

[16] Suzen, Y. B., Huang, P. G., Ashpis, D. E., Volino, R. J., Corke, T. C., Thomas, F. O., Huang, J., Lake, J. P., and King, P. I., 2007, "A Computational Fluid Dynamics Study of Transitional Flows in Low-Pressure Turbines Under a Wide Range of Operating Conditions". ASME J. Turbomach., **129** (3), pp. 527–541.

[17] Walters, D. K. and Leylek, J. H., 2004, "A New Model for Boundary Layer Transition Using a Single-Point RANS Approach". ASME J. Turbomach., **126** (1), pp. 193–202.

[18] Walters, D. K. and Leylek, J. H., 2005, "Computational Fluid Dynamics Study of Wake-Induced Transition on a Compressor-Like Flat Plate". ASME J. Turbomach., **127** (1), pp. 52–63.

[19] Lardeau, S., Leschziner, M. A., and Li, N., 2004, "Modelling Bypass Transition with Low-Reynolds-Number Nonlinear Eddy-Viscosity Closure". Flow Turbul. Combust., **73**, pp. 49–76.

[20] Mayle, R. E. and Schultz, A., 1997, "The Path to Predicting Bypass Transition". ASME J. Turbomach., **119** (3), pp. 405–411.

[21] Lardeau, S. and Leschziner, M. A., 2006, "Modelling of Wake-Induced Transition in Low-Pressure Turbine Cascades". AIAA J., **44** (8), pp. 1854–1865.

[22] Pacciani, R., Marconcini, M., Fadai-Ghotbi, A., Lardeau, S., and Leschziner, M. A., 2009, "Calculation of High-Lift Cascades in Low Pressure Turbine Conditions Using a Three-Equation Model". ASME paper GT2009-59557, (ASME J. Turbomach. to be published).

[23] Wilcox, D. C., 1998, *Turbulence Modeling for CFD*, 2nd edition, DCW Ind. Inc., La Cañada, CA, USA, ISBN 1-928729-10-X.

[24] Arnone, A., Liou, M. S., and Povinelli, L. A., 1992, "Navier–Stokes Solution of Transonic Cascade Flow Using Non–Periodic C–Type Grids". J. Prop. Power, **8** (2), pp. 410–417.

[25] Arnone, A. and Pacciani, R., 1996, "Rotor-Stator Interaction Analysis Using the Navier-Stokes Equations and a Multigrid Method". ASME J. Turbomach., **118** (4), pp. 679–689.

[26] Jameson, A., 1991, "Time Dependent Calculations Using Multigrid with Applications to Unsteady Flows Past Airfoils and Wings". AIAA paper 91–1596.

[27] Lardeau, S., Li, N., and Leschziner, M. A., 2007, "Large Eddy Simulations of Transitional Boundary Layers at High Free-Stream Turbulence Intensity and Implications for RANS Modeling". ASME J. Turbomach., **129** (1), pp. 1–7.

[28] Wissink, J. G. and Rodi, W., 2006, "Direct Numerical Simulations of Transitional Flow in Turbomachinery". ASME J. Turbomach., **128** (4), pp. 668–678.

[29] Menter, F. R., 1992, "Assessment of Higher Order Turbulence Models for Complex Two- and Three-Dimensional Flowfields". NASA TM-103944.

[30] Hoheisel, H., 1990, "Test Case E/CA-6, Subsonic Turbine Cascade T106, Test Cases for Computation of Internal Flows in Aero Engine Components." AGARD-AR-275.

[31] Pacciani, R. and Spano, E., 2006, "Numerical Investigation of the Effect of Roughness and Passing Wakes on LP Turbine Blades Performance". ASME paper GT2006-90221.

[32] Menter, F. R., 1992, "Improved Two-Equation k-ω Turbulence Models for Aerodynamic Flows". NASA TM-103975.

[33] Menter, F. R., 1994, "Two–Equations Eddy Viscosity Turbulence Models for Engineering Applications". AIAA J., **32** (8), pp. 1598–1605.

[34] Chima, R. V., 1996, "A k–ω Turbulence Model for Quasi–Three–Dimensional Turbomachinery Flows". J. Prop. Power, **12** (6), pp. 1176–1179.

[35] Roberts, S. K. and Yaras, M. I., 2005, "Large-Eddy Simulation of Transition in a Separation Bubble". ASME J. Fluids Eng., **128** (2), pp. 232–238.

[36] Michálek, J., Monaldi, M., and Arts, T., 2010, "Aerodynamic Performance of a Very High Lift Low Pressure Turbine Airfoil (T106C) at Low Reynolds and High Mach Number with Effect of Free Stream Turbulence Intensity". ASME paper GT2010-22884.

[37] Coull, J. D., Thomas, R. L., and Hodson, H. P., 2008, "Velocity Distributions for Low Pressure Turbines". ASME paper GT2008-50589.